Space-Quasiperiodic and Time-Chaotic Parametric Patterns in a Magnonic Quasicrystal Active Ring Resonator

Sergei V. Grishin,[1,*] Olga I. Moskalenko,[1] Alexey N. Pavlov,[1] Dmitrii V. Romanenko,[1] Alexandr V. Sadovnikov,[1] Yurii P. Sharaevskii,[1] Ilya V. Sysoev,[1] Tatiana M. Medvedeva,[2] Evgenii P. Seleznev,[3] and Sergei A. Nikitov[4]

[1] *Saratov State University, Saratov 410012, Russia*

[2] *Institute of Higher Nervous Activity and Neurophysiology of RAS, Moscow 117485, Russia*

[3] *Branch of Kotel'nikov Institute of Radioengineering and Electronics, of RAS, Saratov 410019, Russia*

[4] *Kotel'nikov Institute of Radioengineering and Electronics of RAS, Moscow 125009, Russia*

(Received 12 November 2020; revised 26 October 2021; accepted 1 November 2021; published 15 November 2021)

We demonstrate the dissipative spatiotemporal patterns that are generated by an active ring resonator based on a magnonic quasicrystal (MQC) with Fibonacci-type structure. The dissipative patterns are formed through the magnetostatic surface spin-wave (MSSW) parametric decay into exchange spin waves (SWs), temporal dispersion of the ring resonator and amplification. In the spatial domain, the MSSW and SW parametric patterns measured with the help of Brillouin light spectroscopy have the quasiperiodic spatial localization in crests and grooves of the MQC, respectively. In contrast to the optical quasiperiodic parametric spatial conservative solitons, the amplitude profiles of the magnonic quasiperiodic parametric spatial dissipative patterns correspond to the profiles of the crests and grooves of the MQC. In the time domain, the packets of the chaotic parametric pulses, which are analogs of temporal solitons, are generated at each point of the spatial patterns. The chaotic nature of such pulses is confirmed by an estimate of a highest Lyapunov exponent from the experimental time series. The pulse packets are formed through the time-filtering technique using the external microwave (MW) pulses to control a ring gain. It is shown that at a certain duty factor of the external MW pulses, the parametric MSSW pulses have the amplitude and phase profiles corresponding to the profiles of a conservative bright envelope soliton.

DOI: 10.1103/PhysRevApplied.16.054029

I. INTRODUCTION

The spatiotemporal patterns and chaos are the most common natural phenomena that are observed in the open, highly nonequilibrium systems related to the various fields of science: hydrodynamics [1,2], plasma physics [3,4], vacuum electronics [5], chemistry [6,7], biology [8], etc. Both phenomena are the traditional objects of the research in synergetics [9]. In dissipative systems with energy inflow from outside and outflow (dissipation), the dissipative solitons are formed due to a balance between gain and loss [10]. The solitons are asymptotically stable states of a dynamical system, while dynamic chaos is a result of the development of Lyapunov instability. In nonlinear optics and magnonics, the *chaotic solitons* [11–14] and *chaotic multisoliton complexes* [15,16] were discovered in the time domain. The patterns with chaotic spatiotemporal localization were observed in optical experiments with a liquid crystal covered by a feedback loop [17,18] and in semiconductor lasers with saturable absorption [19]. Such chaotic states were called *chaoticons* [17,18].

Besides the chaotic spatiotemporal patterns, the quasiperiodic spatial solitons were theoretically predicted for an optical Fibonacci superlattice at both a signal wave and a second harmonic frequencies [20]. They were obtained through three-wave parametric interaction and spatial dispersion of the Fibonacci superlattice. The parametric spatial patterns were the spatial conservative bright envelop solitons and did not have chaotic temporal dynamics. Their width was comparable with a width of one of the two building blocks of the Fibonacci superlattice.

In nonlinear magnonics, a magnonic quasicrystal (MQC) with Fibonacci-type structure was used in a feedback loop of an active ring resonator to self-generate the dissipative parametric solitons, which are the analogs of the optical temporal solitons [21–24]. The temporal patterns were formed in the time domain due to the parametric decay of a magnetostatic surface spin wave (MSSW) into the parametrically excited exchange spin waves (SWs) and due to temporal dispersion of the active ring resonator. The MSSW had a linear amplification and the exchange

*sergrsh@yandex.ru

SWs were dissipated in the MQC. The MSSW parametric solitons had a noiselike spectrum and the chirped phase profiles, because an instantaneous frequency was changed within the pulses. However, the spatiotemporal dynamics of such parametric patterns has not been investigated. We know of only one paper [25] in which SW localization in a MQC consisting of dipolar coupled permalloy nanowires was investigated. But, here SW localization was studied in the linear case.

In the paper, we demonstrate the spatiotemporal parametric patterns that have both chaotic temporal and quasiperiodic spatial localizations at the MSSW and SW frequencies. In the spatial domain, the amplitude profiles of the quasiperiodic MSSW and SW dissipative patterns correspond to the groove and crest profiles of the MQC, respectively. The packets of the chaotic dissipative temporal solitons with the amplitude and phase profiles corresponding to a conservative bright envelope soliton are generated at each point of the spatial patterns. The temporal solitons possessing such profiles are formed with the help of a time-filtering technique exploiting the microwave (MW) pulses to control a ring gain.

II. EXPERIMENTAL SETUP

A. Magnonic quasicrystal with Fibonacci-type structure

The MQC with Fibonacci-type structure is a quasiperiodic sequence of crests and grooves that are formed on a surface of an yttrium-iron-garnet (YIG) film by the etching technique. The YIG film has a thickness of 7.7 μm, a width of 4 mm, a length of 8 mm, and a saturation magnetization of 1750 G. The width of the grooves is $a_1 = 130$ μm and $2a_1 = 260$ μm. Their height is $h_1 = 5.7$ μm. The width of the crests is $a_2 = 145$ μm and their height h_2 corresponds to the thickness of the YIG film. The quasiperiodic structure with a length of 4.485 mm is constructed on the base of the first six iterations of Fibonacci algorithm: $s_{j+1} = s_{j-1}s_j$, $s_0 = a_2$, $s_1 = a_1$ ($j \geq 1$). Following this algorithm, the quasiperiodic sequence of crests and grooves is given as

$$S = \{a_2a_1a_2 2a_1a_2a_1a_2 2a_1a_2 2a_1a_2a_1a_2 2a_1a_2a_1a_2 \cdot \\ \cdot 2a_1a_2 2a_1a_2a_1a_2 2a_1a_2a_1\}.$$

The MQC with Fibonacci-type structure is both a multiresonant and nonlinear element. It was found [22], that the MQC has a higher density of stop bands in contrast to a magnonic crystal (MC) possessing strict periodicity. This MQC feature allows use of it in a feedback loop of an active ring resonator to control not only the frequency interval between the ring eigenmodes, which determines the temporal dispersion of the ring resonator, but also their intensity. As shown in Ref. [23], the intermode interval is decreased with increasing strength of a biased magnetic field both for the MQC and the MC. However, for the MC this interval is always larger than for the MQC. Besides, the MQC can support parametric decay of the MSSW into exchange SWs [21]. It is well known that the MSSW parametric instability leads to a self-generation of the relaxation-type pulse sequences, when a YIG film without the quasiperiodic structure is contained in the feedback loop of the active ring resonator [26]. However, the filtering properties of the MQC allows control of the amplitude profiles of such pulses and formation from them of the bell-shaped pulses.

B. Magnonic quasicrystal active ring resonator

In Fig. 1, the scheme of an active ring resonator containing the MQC with Fibonacci-type structure, an amplifier, and a variable attenuator is presented. The excitation and detection of the MSSWs propagating in the MQC is realized by the use of two (input and output) microstrip transducers. Each transducer is 30 μm wide and 6 mm long. The distance between them is $L = 4.5$ mm. The external static magnetic field $H_0 = 560$ Oe is in the plane and it is perpendicularly to the direction of the MSSW propagation. The amplifier is a wideband transistor amplifier operating in the 2–4 GHz frequency band. An external MW pulse generator forms the external MW pulses that are used both to synchronize the operation of the MQC active ring resonator with an interferometer included in the Brillouin-light-scattering (BLS) setup and to realize the time filtration of the self-generated dissipative solitons. The BLS setup operates on the Mandelstam-Brillouin scattering of light by inhomogeneities. In our case, such inhomogeneities are

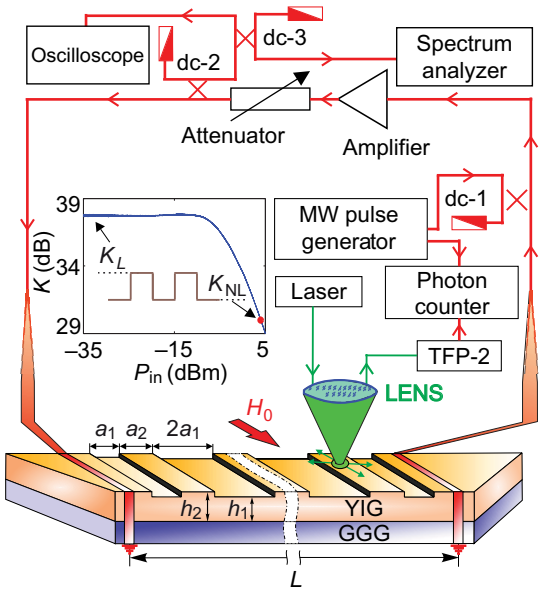

FIG. 1. Scheme of a MQC active ring resonator.

the quasiparticles—*magnons*. The main part of the MW pulse power is applied to the amplifier input and their smaller part enter to the interferometer input. The characteristics of the external and self-generated pulses are measured by a real-time oscilloscope, a spectrum analyzer and a power meter. The variable attenuator controls a ring gain $G = K - A$, where A is the total loss in the ring and K is an amplifier gain.

A nonlinear dependence of the amplifier gain K versus input power P_{in} presented in an insert in Fig. 1 is a key role for the time-filtering method [27]. The amplifier operating in the linear amplification mode has a maximum gain K_L, when $P_{\text{in}} < P_{\text{in}}^{\text{sut}}$ (where $P_{\text{in}}^{\text{sut}} = +0.5$ dBm is an input power at which the output-power saturation mode is achieved). The peak power of the external MW pulses P_{ext} (see red circle in the insert in Fig. 1) is set higher than $P_{\text{in}}^{\text{sut}}$, when the nonlinear gain K_{NL} is much smaller than the K_L. Thus, the MW pulses modulate both the amplifier gain and the ring gain. In the time intervals corresponding to the external MW pulses, when the amplifier gain is equal to K_{NL}, the dissipative solitons are not self-generated. In contrast, in the pauses between the MW pulses, when the amplifier gain is equal to K_L, the dissipative solitons are self-generated.

The main advantage of the proposed method of the ring gain modulation by saturating the microwave amplifier in comparison with the breaking of the ring by a microwave switch [28] is the lower level of the generator's noise in the pauses between the dissipative solitons. In the generator scheme with the microwave switch, an amplifier operates in the linear amplification mode and its own noise level will always be higher than the analogous noise level of an amplifier operating in the output-power saturation mode. Moreover, the proposed method always ensures the presence of a signal at the amplifier input. Such an operation mode of some solid-state microwave amplifiers is recommended by the manufacturers for the reasons of reliability of their operation.

The external MW pulses are also fed to the interferometer input of the BLS setup in order to start the process of counting photons reflected from the MQC. The counting of the reflected photons starts in the pauses between the MW pulses, when the dissipative parametric solitons are self-generated in the active ring resonator. A carrier frequency of the external MW pulses is set outside the MSSW frequency band, but within the amplifier frequency band. This is necessary for the frequency separation of the spectra of both pulse signals and for the subsequent frequency filtering of the external MW pulses.

III. EXPERIMENTAL RESULTS AND DISCUSSION

A. Microwave spectroscopy

In the microwave experiment, the parametric pulse trains are measured only at the MSSW frequencies for two values of G. One of them ($G = 0$) corresponds to the single-mode generation and the other ($G = 2.1$ dB) corresponds to the multimode generation. In both cases, a carrier frequency of the external MW pulses $f_{\text{ext}} = 2$ GHz is located outside the MSSW frequency band but inside the amplifier frequency band. The pulse width and peak power are chosen in such a way that each MW pulse can suppress one parametric pulse of the sequence. The external MW pulses have the width $T_{d2} = 800$ ns and a repetition interval $T_{r2} = 10.752$ μs that determines a time interval between the parametric pulse packets.

In Fig. 2, the frequency and temporal characteristics of the parametric pulses measured in the single-mode generation are demonstrated. As shown in Fig. 2(a), a carrier frequency of the parametric pulse train is $f_{\text{osc1}} = 3241.3$ MHz that coincides with a central frequency of a MQC first passband. The generated signal has a noiselike spectrum [see an insert in Fig. 2(a)] because it average power $P_{\text{av}} = +4.3$ dBm is significantly greater than a three-wave parametric threshold ($P_{\text{th}} = -18$ dBm). In the time domain [see Fig. 2(b)], the parametric pulse train contains the packets of four parametric pulses with a duration $T_{d1} = 440$ ns measured at the 0.7 level of the peak amplitude. The parametric pulses are formed after many rounds of the signal around the ring because the pulse width significantly exceeds a signal trip time around the ring ($\tau_r \sim 100$

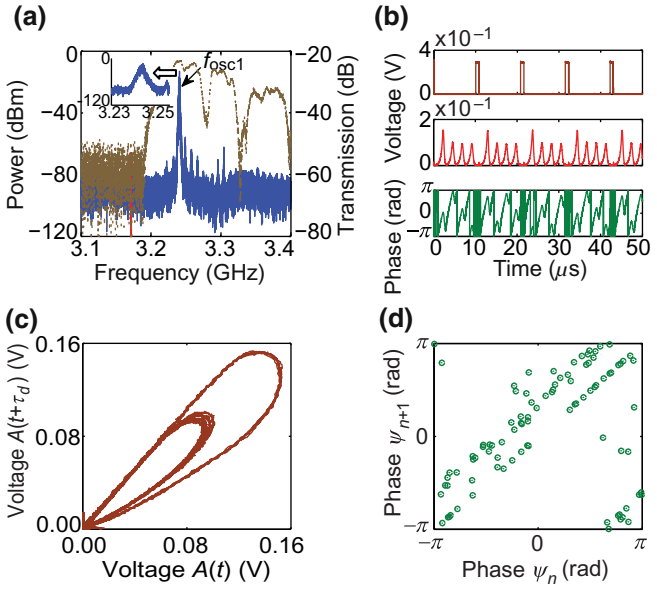

FIG. 2. Characteristics of the dissipative solitons generated in the single-mode regime under the external MW pulses: (a) the microwave power spectrum (solid line) of the dissipative solitons, (b) the time series of the envelope of the MW pulses (upper panel), the dissipative solitons (middle panel) and their phase profiles (lower panel), (c) the projections of a phase portrait on the parameter plane $[A(t), A(t+\tau_d)]$, where $\tau_d = 2\tau_r$, and (d) the iteration diagram of the envelope phase. In (a), the MQC transmission is marked with a dashed line.

ns). The first parametric pulse of each packet is generated in a nonstationary mode and has a significantly higher amplitude than the subsequent pulses generated in a stationary mode. It is explained that the SWs parametrically excited by the MSSW pulses of a previous packet have the time to return back to the initial nonexcited state and do not influence the first MSSW pulse of a following packet.

As shown in Fig. 2(c), the attractor of the parametric pulse train is similar to the limit cycle of double period. One of them corresponds to the "gigantic" amplitude pulses, and the other is determined by the smaller amplitude pulses, which are generated in the stationary mode. However, the phase trajectories of the attractor do not exactly repeat each other that indicates the possibility of chaotic nature of the generated pulses.

In Fig. 2(d), an iteration phase diagram shows a violation of the phase synchronization of the harmonics of a modulation frequency f_{am}, which is a result of a modulation of the MSSW by the SWs. The phase values are determined on the attractor in the Poincaré section. The amplitude values of the envelope lying on the secant plane of the attractor are assigned the values of the phase calculated using the Hilbert transform. The iteration phase diagram clearly demonstrates the violation of the phase synchronization of the harmonics of f_{am} that may be connected with the chaotic dynamics.

The self-generated parametric pulses are the analogs of optical temporal bright envelope solitons because temporal dispersion of the ring resonator takes part in their formation. It was theoretically shown [23] that the active ring resonator is an artificial distributed medium with temporal dispersion, if a resonant element is used in a feedback loop. In our case, the MQC is such a resonant element. It affects the amplitude profile of parametric pulses, making them bell shaped. The phase profiles of parametric pulses calculated with the help of the Hilbert transform have a clear chirp corresponding to the chirped dissipative solitons [10].

The increase of the ring gain to $G = 2.1$ dB leads to the multimode generation (see Fig. 3). In this case, the packets of parametric pulses are formed in the same manner as in the single-mode generation [Fig. 2(b)], but the parametric pulse power is increased and their phase profiles are changed. To form the parametric pulses with the amplitude and phase profiles similar to the bright conservative envelope solitons, a duty factor q of the MW pulses is varied. At $q = 15$, the average power is increased to $P_{av} = +5.6$ dBm and concentrated basically at the frequencies f_{osc1}, f_{osc2}, and f_{osc3} that correspond to three ring eigenmodes. The frequencies $f_{osc2} = 3268.2$ MHz and $f_{osc3} = 3297.3$ MHz are located near the central frequencies of the MQC first and second passbands [see Fig. 2(a)]. Each packet of the train contains the eight parametric pulses with rapidly changing phase.

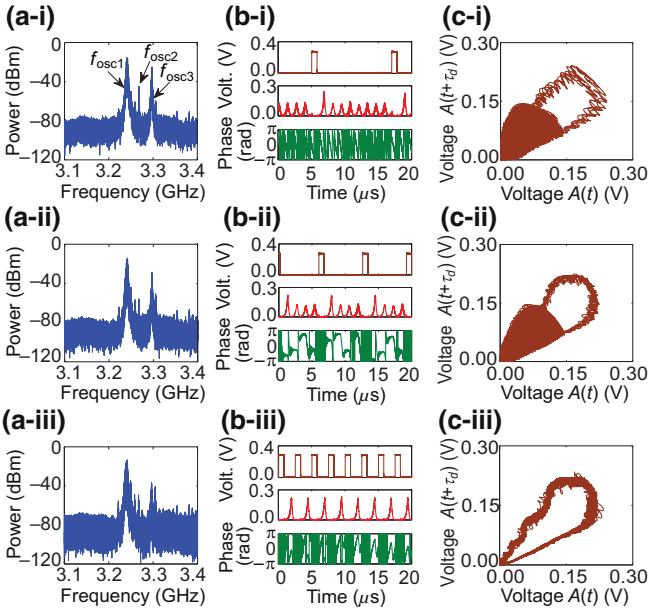

FIG. 3. Characteristics of the dissipative solitons generated in the multimode regime at three values of the duty factor q of the external MW pulses: (a-i), (b-i), (c-i) 15; (a-ii), (b-ii), (c-ii) 8.25 and (a-iii), (b-iii), (c-iii) 3.125. In (a-i), (a-ii), and (a-iii) the microwave power spectra of the dissipative solitons, in (b-i), (b-ii), and (b-iii) the time series of the envelope of the MW pulses (upper panel), the dissipative solitons (middle panel), and their phase (lower panel), in (c-i), (c-i), and (c-iii) the projections of a phase portrait on the parameter plane $[A(t), A(t+\tau_d)]$.

The further decrease of q leads to the signal suppression at the frequencies f_{osc2} and f_{osc3} and to the phase-profile transformation. At $q = 8.25$, the phase profiles of four parametric pulses are flat across their width and are similar to the phase profile of the bright conservative envelope soliton [29]. In this case, the power level $P_{av} = +6.2$ dBm is the bright envelope soliton threshold. At $q = 3.125$, the train consists only of the "gigantic" pulses with $P_{av} = +7.4$ dBm. Now, the main power is concentrated only at the frequency f_{osc1}. The pulse phase profiles have clear chirp that corresponds again to the chirped dissipative solitons [see Fig. 2(b)].

Following the results presented in Figs. 3(c-i) and 3(c-ii), the attractor structure for the small amplitudes becomes strongly "blurred," because the envelope of the smaller pulses fast oscillates. In contrast, the envelope of the "gigantic" pulses do not have such a variation. At $q = 3.12$ [see Fig. 3(c-iii)] the attractor structure becomes clearly distinguishable at all amplitude values, when the generation of the smaller amplitude pulses is absent.

The chaotic nature of the generated dissipative solitons is evidenced by the estimates of the highest Lyapunov exponent (HLE) from the experimental time series. To estimate the HLE, two methods are used [30,31]. One of them [31] is adapted for short time series. The results

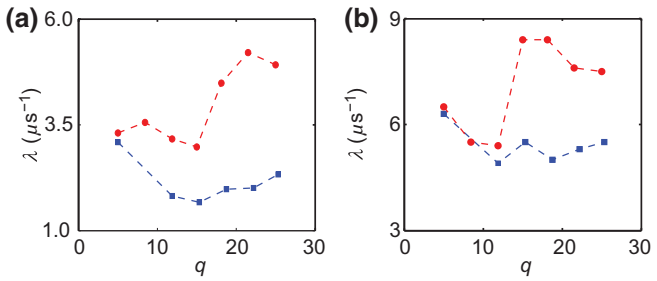

FIG. 4. Dependences of the highest Lyapunov exponent λ on the duty factor q calculated based on the experimental time series by two methods: (a) Wolf method and (b) Rosenstein method. Circles correspond to the single-mode and squares correspond to the multimode generation regime. For both methods, the calculations are performed for the embedding dimension $D_{\text{emb}} = 9$.

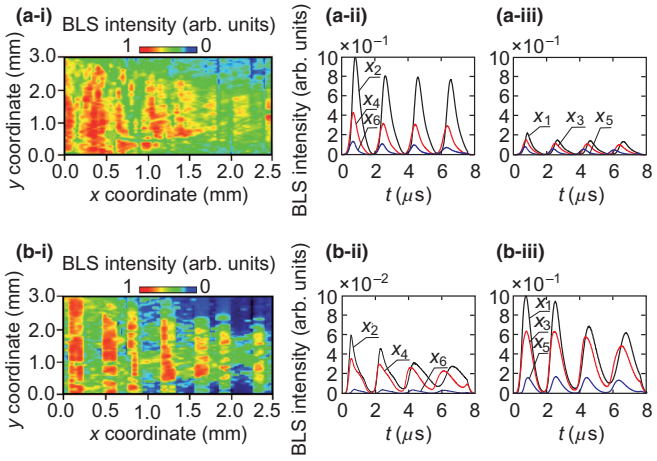

FIG. 5. The spatial (a-i), (b-i) and temporal (a-ii), (a-iii), (b-ii), (b-iii) distributions of the square of the magnetization amplitude measured (a) at the MSSW frequency $f_{\text{osc1}} = 3241.3$ MHz and (b) at the SW frequency $f_{\text{osc1}}/2$. In both cases, the temporal distributions are obtained for grooves (a-ii), (b-ii) and crests (a-iii), (b-iii). The symbols $x_1 - x_6$ correspond to six values of the spatial coordinate: $x_1 = 0.2$ mm, $x_2 = 0.4$ mm, $x_3 = 0.65$ mm, $x_4 = 0.75$ mm, $x_5 = 1.9$ mm, $x_6 = 2.15$ mm. Even symbols correspond to the grooves, and odd symbols correspond to the crests.

of such assessments are shown in Fig. 4. It can be seen that both methods give the positive values of HLE for both the single-mode and multimode generation, that accurately indicate the chaotic dynamics. Differences between the results can be caused by the features of characterizing the instability of the phase-space trajectories for noisy data sets, especially under external forces. For both generation modes, the values of HLE practically coincide only for small values of q, when the multimode generation is significantly suppressed. The increase of q of the external MW pulses leads to the influence of several ring eigenmodes on the parametric pulse generation. As a result, the HLE for the multimode generation becomes smaller than for the single-mode generation.

B. BLS spectroscopy

For the BLS experiment, the multimode generation at $q = 8.25$ is chosen. However, the chaotic dynamics of the solitonlike pulses is a factor that can limit the investigation of their spatiotemporal dynamics using the BLS setup. At the same time, the deviations of the amplitude and pulse repetition interval are characterized by relatively small values, which do not exceed 10% of the maximum value. Within these deviations, the study of the spatiotemporal dynamics of the parametric patterns is acceptable.

Figure 5 demonstrates the spatial and temporal distributions of the light radiation intensity, that are proportional to the square of the magnetization amplitude. These distributions are measured at both the MSSW and SW frequencies. The spatial map of the MSSW magnetization distribution measured at the frequency f_{osc1} [see Fig. 5(a-i)] corresponds to the superposition of the MSSW odd (first and third) width modes propagating in a ferromagnetic waveguide [32]. However, in contrast to the spatial distribution of the MSSW magnetization observed in a homogeneous ferromagnetic film placed in a feedback loop of an active ring resonator [33], the MSSW magnetization in the MQC active ring resonator has clear maxima localized only in the MQC grooves. Besides, as follows from Fig. 5(b-i), the SW excitation at a frequency $f_{\text{osc1}}/2$ is also observed in the region of the MSSW first and third width modes. However, in contrast to the MSSWs, the maxima of the SW magnetization are localized only in the crests of the MQC.

As follows from Fig. 5, the packets of the MSSW and SW pulses are formed at each spatial point of the crests and grooves. Each packet consists of four pulses, one of which (the first pulse) has the largest amplitude. For the MSSW pulses [see Figs. 5(a-ii) and 5(a-iii)], their amplitudes are maximum in grooves and minimum in crests. For the SW pulses [see Figs. 5(b-ii) and 5(b-iii)], the situation is exactly the opposite. The amplitudes of the SW pulses are maximum in crests and minimum in grooves. Moreover, the amplitudes of all pulses are decreased with increasing a distance from the input microstrip, but the number of pulses in a packet remains the same for both MSSWs and SWs. It should be noted that similar spatial localization of parametrically interacting waves was theoretically predicted earlier for the optical Fibonacci superlattice, in which the quasiperiodic sequences of spatial parametric bright envelope solitons were formed [20]. However, such quasiperiodic parametric solitons were the conservative solitons, which had not a chaotic temporal dynamics.

IV. CONCLUSION

In conclusion, we note that similar spatiotemporal patterns can be obtained not only in magnonics, but also in optics, hydrodynamics, and plasma, if the dissipative system with the wave turbulence appearing due to parametric wave instability is described by the Vyshkind-Rabinovich model [34], and the spatial ordering of the medium is changed according to a quasiperiodic law. The obtained results may be of interest to specialists involved in the creation of pulse sources for microwave and optical communications.

ACKNOWLEDGMENTS

The mathematical processing of time series is supported by the Russian Foundation for Basic Research (Project No. 19-02-00075). The development of a generator layout and experimental studies of the parametric patterns are supported by the Russian Science Foundation (Project No. 19-79-20121).

[1] A. Kudrolli and J. P. Gollub, Patterns and spatiotemporal chaos in parametrically forced surface waves: A systematic survey at large aspect ratio, Phys. D **97**, 133 (1996).

[2] A. Kudrolli and J. P. Gollub, Localized spatiotemporal chaos in surface waves, Phys. Rev. E **54**, R1052 (1996).

[3] T. Nagasawa, Chaotic phenomena of a periodic ion-acoustic soliton system, Phys. Plasmas **6**, 3471 (1999).

[4] H.-L. Zhen, B. Tian, Y.-F. Wang, and D.-Y. Liu, Soliton solutions and chaotic motions of the Zakharov equations for the Langmuir wave in the plasma, Phys. Plasmas **22**, 032307 (2015).

[5] D. I. Trubetskov, E. S. Mchedlova, V. G. Anfinogentov, V. I. Ponomarenko, and N. M. Ryskin, Nonlinear waves, chaos and patterns in microwave electronic devices, Chaos **3**, 358 (1996).

[6] W. Y. Tam, J. A. Vastano, H. L. Swinney, and W. Horsthemke, Regular and Chaotic Chemical Spatiotemporal Patterns, Phys. Rev. Lett. **61**, 2163 (1988).

[7] D. G. Miguez, M. Dolnik, I. Epstein, and A. P. Munuzuri, Interaction of chemical patterns in coupled layers, Phys. Rev. E **84**, 046210 (2011).

[8] A. J. Koch and H. Meinhardt, Biological pattern formation: From basic mechanisms to complex structures, Rev. Mod. Phys. **66**, 1481 (1994).

[9] H. Haken, *Advanced Synergetics* (Springer, Berlin, Heidelberg, 1985).

[10] N. Akhmediev and A. Ankiewicz, *Dissipative Solitons: From Optics to Biology and Medicine* (Springer-Verlag, Berlin, 2008).

[11] S. R. Bolton and M. R. Acton, Quasiperiodic route to chaos in the Kerr-lens mode-locked Ti:sapphire laser, Phys. Rev. A **62**, 063803 (2000).

[12] N. Akhmediev, J. M. Soto-Crespo, and G. Town, Pulsating solitons, chaotic solitons, period doubling, and pulse coexistence in mode-locked lasers: Complex Ginzburg-Landau equation approach, Phys. Rev. E **63**, 056602 (2001).

[13] E. N. Beginin, S. V. Grishin, and Y. P. Sharaevsky, Generation of a stationary train of chaotic soliton-like microwave pulses in self-oscillating ring systems with a ferromagnetic thin film, JETP Lett. **88**, 647 (2008).

[14] Z. Wang, A. Hagerstrom, J. Q. Anderson, W. Tong, M. Wu, L. D. Carr, R. Eykholt, and B. A. Kalinikos, Chaotic Spin-Wave Solitons in Magnetic Film Feedback Rings, Phys. Rev. Lett. **107**, 114102 (2011).

[15] S. V. Grishin, B. S. Dmitriev, O. I. Moskalenko, V. N. Skorokhodov, and Y. P. Sharaevskii, Self-generation of chaotic dissipative multisoliton complexes supported by competing nonlinear spin-wave interactions, Phys. Rev. E **98**, 022209 (2018).

[16] A. S. Bir, S. V. Grishin, O. I. Moskalenko, A. N. Pavlov, M. O. Zhuravlev, and D. O. Ruiz, Experimental Observation of Ultrashort Hyperchaotic Dark Multisoliton Complexes in a Magnonic Active Ring Resonator, Phys. Rev. Lett. **125**, 083903 (2020).

[17] N. Verschueren, U. Bortolozzo, M. G. Clerc, and S. Residori, Spatiotemporal Chaotic Localized State in Liquid Crystal Light Valve Experiments with Optical Feedback, Phys. Rev. Lett. **110**, 104101 (2013).

[18] N. Verschueren, U. Bortolozzo, M. Clerc, and S. Residori, Chaoticon: Localized pattern with permanent dynamics, Phil. Trans. R. Soc. A. **372**, 20140011 (2014).

[19] H. Vahed, F. Prati, M. Turconi, S. Barland, and G. Tissoni, Periodic and chaotic solitons in a semiconductor laser with saturable absorber, Phil. Trans. R. Soc. A. **372**, 20140016 (2014).

[20] C. B. Clausen, Y. S. Kivshar, O. Bang, and P. L. Christiansen, Quasiperiodic Envelope Solitons, Phys. Rev. Lett. **83**, 4740 (1999).

[21] S. V. Grishin, E. N. Beginin, Y. P. Sharaevskii, and S. A. Nikitov, Dissipative soliton generation in an active ring resonator based on magnonic quasicrystal with fibonacci type structure, Appl. Phys. Lett. **103**, 022408 (2013).

[22] S. V. Grishin, E. N. Beginin, M. A. Morozova, Y. P. Sharaevskii, and S. A. Nikitov, Self-generation of dissipative solitons in magnonic quasicrystal active ring resonator, J. Appl. Phys. **115**, 053908 (2014).

[23] S. V. Grishin, E. N. Beginin, M. A. Morozova, Y. P. Sharaevskii, and S. Nikitov, Self-generation of parametric soliton-like pulses in a magnonic quasicrystal active ring resonator, IEEE Trans. Magn. **50**, 4006204 (2014).

[24] S. V. Grishin, T. M. Golova, M. A. Morozova, D. V. Romanenko, E. P. Seleznev, I. V. Sysoev, and Y. P. Sharaevskii, Chaotic parametric soliton-like pulses in ferromagnetic-film active ring resonators, JETP **121**, 623 (2015).

[25] F. Lisiecki, J. Rychły, P. Kuswik, H. Glowinski, J. W. Kłos, F. Groß, N. Träger, I. Bykova, M. Weigand, M. Zelent, E. J. Goering, G. Schütz, M. Krawczyk, F. Stobiecki, J. Dubowik, and J. Gräfe, Magnons in a Quasicrystal: Propagation, Extinction, and Localization of Spin Waves in Fibonacci Structures, Phys. Rev. Appl. **11**, 054061 (2019).

[26] V. E. Demidov and N. G. Kovshikov, Mechanism for the appearance and randomization of the self-modulation of high-intensity spin waves, Tech. Phys. **44**, 960 (1999).

[27] S. V. Grishin, E. V. Zar'kova, and Y. P. Sharaevskii, Generation of chaotic microwave pulses in broadband self-oscillating ring system with ferromagnetic film under the action of external pulse-modulated microwave signal, Tech. Phys. Lett. **37**, 237 (2011).

[28] B. A. Kalinikos, N. G. Kovshikov, and C. E. Patton, Decay Free Microwave Magnetic Envelope Soliton Pulse Trains in Yttrium Iron Garnet Thin Films, Phys. Rev. Lett. **78**, 2827 (1997).

[29] J. M. Nash, P. Kabos, R. Staudinger, and C. E. Patton, Phase profiles of microwave magnetic envelope solitons, J. Appl. Phys. **83**, 2689 (1998).

[30] A. Wolf, J. B. Swift, H. L. Swinney, and J. A. Vastano, Determining lyapunov exponents from a time series, Physica (Amsterdam) **16D**, 285 (1985).

[31] M. T. Rosenstein, J. J. Collins, and C. J. De Luca, A practical method for calculating largest Lyapunov exponents from small data sets, Phys. D **65**, 117 (1993).

[32] T. W. O'Keefe and R. W. Patterson, Magnetostatic surface-wave propagation in finite samples, J. Appl. Phys. **67**, 4886 (1978).

[33] D. V. Romanenko, S. V. Grishin, A. V. Sadovnikov, Yu. P. Sharaevskii, and S. A. Nikitov, Spatial and temporal dynamics of dissipative parametric solitons in a ferromagnetic film active ring resonator, IEEE Trans. Magn. **50**, 4006304 (2014).

[34] S. Y. Vyshkind and M. I. Rabinovich, The phase stochastization mechanism and the structure of wave turbulence in dissipative media, Sov. Phys. JETP **44**, 292 (1976).